Synthesis and Characterization of Highly Ordered Ni-MCM-41 Mesoporous Molecular Sieves

Yanhui Yang, Sangyun Lim, Guoan Du, Yuan Chen, Dragos Ciuparu, and Gary L. Haller*

Department of Chemical Engineering, Yale University, New Haven, Connecticut 06520

Received: December 19, 2004; In Final Form: April 9, 2005

Highly ordered Ni-MCM-41 samples with nearly atomically dispersed nickel ions were prepared reproducibly and characterized. Similar to the Co-MCM-41 samples, the pore diameter and porosity can be precisely controlled by changing the synthesis surfactant chain length. Nickel was incorporated by isomorphous substitution of silicon in the MCM-41 silica framework, which makes the Ni-MCM-41 a physically stable catalyst in harsh reaction conditions such as CO disproportionation to single wall carbon nanotubes or CO_2 methanation. X-ray absorption spectroscopy results indicate that the overall local environment of nickel in Ni-MCM-41 was a tetrahedral or distorted tetrahedral coordination with surrounding oxygen anions. Hydrogen TPR revealed that our Ni-MCM-41 samples have high stability against reduction; however, compared to Co-MCM-41, the Ni-MCM-41 has a lower reduction temperature, and both the H_2-TPR and in situ XANES TPR reveal that the reducibility of nickel is not clearly correlated with the pore radius of curvature, as in the case of Co-MCM-41.[1] This is probably a result of nickel being thermodynamically more easily reduced than cobalt. The stability of the structural order of Ni-MCM-41 has been investigated under SWNT synthesis and CO_2 methanation reaction conditions as both require catalyst exposure to reducing environments leading to formation of metallic Ni clusters. Nitrogen physisorption and XRD results show that structural order was maintained under both SWNT synthesis and CO_2 methanation reaction conditions. EXAFS results demonstrate that the nickel particle size can be controlled by different prereduction temperatures but not by the pore radius of curvature as in the case of Co-MCM-41.

Introduction

The idea of introducing transition elements into zeolites to tune their catalytic properties, such as activity and selectivity, is one of the main themes of heterogeneous catalytic research. However, these materials are restricted to structures having pore diameters less that 1.3 nm. Large organic molecules are sterically hindered in zeolites, which limits the use of these catalysts to applications involving small organic compounds. MCM-41 mesoporous molecular sieves were patented by Mobil scientists more than a decade ago,[2,3] and transition metal incorporated MCM-41catalysts have been investigated extensively since then.[4−7] These materials present an opportunity for the design of catalytically active sites inside uniform channels with controllable nano-order pore diameter, which extends up to 10 nm. The mesoporous molecular sieves bridge the gap between crystalline zeolites and amorphous silica in terms of pore diameter and pore size distribution and make possible chemical reactions which require larger organic compounds, for example, photooxidation of carotenoids,[8] dimerization, and isomerization, etc.[9]

Supported nickel catalysts have been used in many applications, such as desulfurization,[10,11] hydrogenation of aromatics.[12,13] and selective oxidation of aromatic hydrocarbons.[14−16] Nickel also shows good activity for CO_2 methanation, as recently reported.[17−19] Mesoporous nickelsilicate membranes on alumina supports have been successfully prepared and their permeability and catalytic behavior were studied for the oxidation of styrene and benzene.[20,21] These studies revealed that the oxidation of styrene with membrane reactors results in the formation of epoxy ethyl benzene, while the conventional batch reactor gives benzaldehyde selectively. The activity and selectivity of nickelsilicate membrane catalysts have been correlated with their mesoporous structure, permeation properties, and characteristics inherent to membrane reactor.

Nickel and nickel cobalt alloys have also been used as catalysts for the preparation of single wall carbon nanotubes (SWNT),[22−27] and carbon fibers prepared by pyrolysis of methane as reported by Takehira et al.[28]

Cobalt incorporated MCM-41 is known to be a good catalyst for the synthesis of SWNT.[29] As a next neighbor of cobalt in the periodic table of elements, well-dispersed nickel nanoparticles inside MCM-41 mesopores are expected to result from reduction of Ni-MCM-41 by analogy to Co-MCM-41.[4,30]

In this contribution, highly ordered nickel incorporated MCM-41 samples with different pore diameters and different nickel concentrations were prepared, and were used as catalysts for CO_2 methanation and catalytic templates to synthesize SWNT. Various characterization techniques such as nitrogen physisorption, XRD, TEM, hydrogen temperature programmed reduction (TPR), and X-ray absorption spectroscopy were used to characterize the physiochemical properties of Ni catalytic templates used for the synthesis of SWNT. The physical properties of Ni-MCM-41 catalysts during CO_2 methanation were investigated as well. The present paper will focus on the similarities and differences between nickel and cobalt resulting from their neighboring position in the periodic table of elements, which is expected to impart similar characteristics in both their physical and chemical properties. A detailed description of

* Author to whom correspondence should be addressed. E-mail: gary.haller@yale.edu.

10.1021/jp044227i CCC: $30.25
Published on Web 06/16/2005

cobalt incorporated MCM-41 may be found elsewhere.[4] A detailed comparison of catalytic performance of Ni-MCM-41 and Co-MCM-41 for SWNT synthesis has been submitted elsewhere.[31]

Experimental Section

Materials. Silica synthesis sources used were Cab-O-Sil M-5 from Cabot Co (surface area: 200 m^2/g) and tetramethylammonium silicate (19.9% silica, Aldirch). The nickel source was $Ni(NO_3)_2 \cdot 6H_2O$ (Sigma-Aldrich Chemical Co.). Quaternary ammonium surfactants, $C_nH_{2n+1}(CH_3)_3NBr$, were used to form the template with $n = 12$, 14, 16 (Sigma-Aldrich Co.) and with $n = 10$ (American Tokyo Kasei). The surfactant solutions were prepared by ion-exchanging the 29 wt % $C_nH_{2n+1}(CH_3)_3NBr$ aqueous solution with equal molar exchange capacity of Amberjet-4400(OH) ion-exchange resin (Sigma Co.) by overnight batch mixing. The antifoaming agent was Antifoam A (Sigma Co.), which is a silane polymer alkyl terminated by methoxy groups. Acetic acid (Fisher Scientific) was used for pH adjustment of the synthesis solution. In the text hereafter specific samples are designated by the alkyl chain length of the surfactant used (e.g., C16-Ni-MCM-41).

Synthesis. The preparation process is exemplified with the sample C16-Ni-MCM-41. The surfactant solution was first prepared. The powder of cetyltrimethylammonium bromide ($CTMA \cdot Br$, 20.0 g) was dissolved in deionized water (80.0 g) to make a 20.0 wt % solution. Then Amberjet 4400 OH anion-exchange resin (50 mL at the ratio of 1 mmol surfactant/mL resin) was added into the solution to exchange Br ions with OH ions. The ion-exchange process was performed overnight under vigorous agitation. The resulting solution was filtered and ready for use. The fumed silica Cab-O-Sil (2.5 g) was added to the tetramethylammonium silicate aqueous solution (10.4 g) and the mixture was stirred vigorously for half an hour. Approximately 51 mL of deionized water was added to improve mixing. The nickel aqueous solution (2 wt % $Ni(NO_3)_2 \cdot 6H_2O$) was added and the solution was stirred for another 30 min. Two drops of antifoam agent (0.2 wt % of surfactant) was added, followed by addition of the surfactant ($C_{16}H_{33}(CH_3)_3N \cdot OH$ 20 wt %) solution (28.7 g). The pH was adjusted to 11.5 by adding acetic acid. The final reactant molar ratios were 0.29 SiO_2 (from $TMA \cdot SiO_2$):0.71 SiO_2 (from Cab-O-Sil):0.27 surfactant:0.01 Ni:86 water. After additional mixing for about 120 min, this synthesis solution was poured into a polypropylene bottle and placed in an autoclave at 373.2 K for 6 days. After the solution was cooled to room temperature, the resulting solid was recovered by filtration, washed with deionized water, and dried under ambient conditions. The predried solid was heated at a constant rate from room temperature to 813.2 K over 20 h under He and held for 1 h under the same conditions, followed by calcination at 813.2 K for 5 h with air to remove the residual surfactant. Because the preparation process may cause some loss of Ni and silica in the byproducts, the final Ni content was determined by ICP analysis at Galbraith Laboratories, Inc. An impregnated Ni supported on MCM-41 (pure silica) sample was prepared for comparison only, and is denoted as Ni/MCM-41.

Nickel aluminate, as a reference compound, was synthesized according to a method published elsewhere.[32] Stoichiometric 1:1 of Ni to Al from 21.2 g of Ni L^{-1} of nickel nitrate solution and 10.7 g of Al L^{-1} of aluminum nitrate solution were mixed under vigorous stirring, and NH_4OH solution was added dropwise with continuous stirring to obtain a pH of about 8.0. The precipitate formed was washed thoroughly with deionized water until free of nitrate and ammonium ions and dried at 373 K for 72 h, followed by calcination in air at 1273 K for 4 h. The X-ray diffraction was measured to confirm that the powder is a mixture of nickel aluminate and nickel oxide.

Characterization. *Nitrogen Physisorption.* Nitrogen adsorption−desorption isotherms were measured at 77 K with a static volumetric instrument Autosorb-3b (Quanta Chrome). Prior to measurement, the samples were outgassed at 473 K to a residual pressure below 10^{-4} Torr. A Baratron pressure transducer (0.001−10 Torr) was used for low-pressure measurements. The pore size distributions were calculated from the desorption isotherms with the BJH method.[33]

X-ray Diffraction (*XRD*). X-ray diffraction measurements were performed with a Schimadzu X-ray diffractometer (Cu Kα, $\lambda = 0.154$ nm, 40 KV, 30 mA) to check if they have the characteristic hexagonal pore structure for both the fresh Ni-MCM-41 catalysts and after reaction.

High-Resolution Transmission Electron Microscopy (*HR-TEM*). HR-TEM, as a complementary technique, was used to confirm the structure and pore size of Ni-MCM-41 catalysts; HR-TEM was performed on a Tecnai F20 200 kV microscope from Philips.

X-ray Absorption. X-ray absorption data of Ni-MCM-41 were measured at the Ni K edge (8333 eV) with use of a double flat Si (220) as the monochromator crystal at beam line X10C, National Synchrotron Light Source, Brookhaven National Laboratory. Approximately 200 mg of Ni-MCM-41 sample was pressed into self-supporting wafers and placed in a stainless steel cell; incidence and transmission intensity of the X-ray beam were measured by ion chambers filled with pure nitrogen. EXAFS in the transmission mode was recorded from 200 eV below to 900 eV above the Ni K edge. The spectra collected were analyzed with the UWXAFS analysis package.[34] The theoretical EXAFS functions for different nickel species (Ni and NiO) generated by the FEFF6 program were used to fit the experimental data to calculate the Ni−Ni and Ni−O first shell coordination numbers.[35] Details of the experimental procedure are given elsewhere.[6]

Hydrogen Temperature-Programmed Reduction (*H_2-TPR*). The reducibility and the stability of Ni-MCM-41 samples prepared were investigated by a temperature-programmed reduction technique using a thermal conductivity detector (TCD) of a gas chromatograph (6890 plus, Agilent). Approximately 200 mg of each sample was loaded into a quartz cell. Prior to each TPR run, the sample cell was purged by ultra zero grade air at room temperature, then the temperature was increased to 773 K at 5 K/min, soaked for 1 h at the same temperature, and cooled to room temperature. This procedure produces a clean surface before running the TPR. The gas flow was switched to 5 vol % of hydrogen in argon balance, and the baseline was monitored until stable. After baseline stabilization, the sample cell was heated at 5 K/min and held for 1 h at 1173 K to ensure complete nickel reduction. An acetone trap was installed between the sample cell and the TCD to condense water produced by sample reduction.

SWNT Synthesis. The detailed experimental procedure of CO disproportionation is described elsewhere.[29]

CO_2 Methanation. Catalytic CO_2 methanation was conducted at atmospheric pressure in a fixed-bed down-flow quartz reactor in the temperature range of 373 to 873 K. The diameter of the quartz reactor is approximately 10 mm. The reactor was heated in a 5 in. id tube furnace controlled by a programmable temperature controller. All the gases were controlled by calibrated mass flow controllers. The reactants of H_2 and CO_2 were mixed at a constant ratio $H_2/CO_2 = 4$ and a constant flow

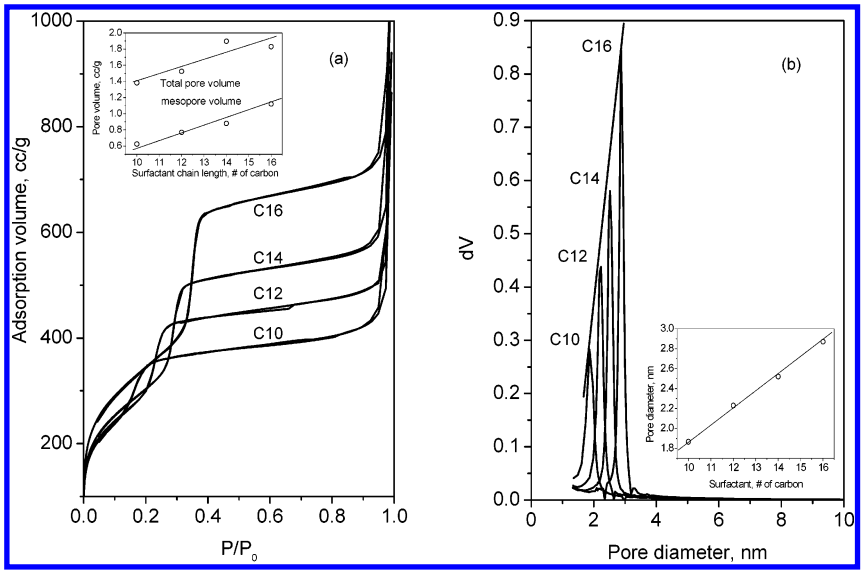

Figure 1. Nitrogen physisorption results of C10−C16 Ni-MCM-41 samples: (a) adsorption/desorption isotherms (inset: correlation of total pore volume and mesopores volume with the surfactant chain length) and (b) pore size distribution (inset: correlation between the pore diameter and the surfactant chain length).

rate of 32 mL/min balanced by ultrahigh purity helium. The amount of catalyst was 100 mg. Prior to each reaction run, the sample was heated to 773 K at 5 K/min, purged by ultra zero grade air, soaked for 1 h at the same temperature to clean the surface, and then prereduced in hydrogen at 973 K for 30 min. The feed and products were analyzed by an on-line programmable gas chromatograph (HP 6890) equipped with TCD and Hayesep D column (100/120 mesh, 20 ft) and Hayesep T column (100/120 mesh, 5 ft).

Results and Discussion

Fresh Ni-MCM-41 Samples (before reaction). Nitrogen physisorption was conducted as the primary measurement to compare the structure of Ni-MCM-41. If the pores in the calcined sample have a uniform diameter, the sample should ideally show a step increase of infinite slope in the adsorption isotherm due to the capillary condensation at a characteristic relative pressure. Figure 1 shows the nitrogen physisorption results of C10 to C16 Ni-MCM-41 catalysts with constant nickel concentration (1.0 wt %). All samples exhibit a sharp capillary condensation step in the adsorption isotherms, indicating highly ordered Ni-MCM-41 catalysts were prepared successfully regardless of the surfactant chain length, which is quite similar to the results of Co-MCM-41 published elsewhere.[4] All samples also exhibit a step increase at around a relative pressure of 0.9−1 due to the filling of interparticle macropores. The high adsorption volume of nitrogen of all samples indicates high surface area; the multipoint BET calculation shows the surface area is around 1200 m^2/g. Very narrow pore size distributions can be found for samples prepared with different alkyl chain lengths. The full width at half-maximum (fwhm) is about 0.13 nm for the best sample. The pore diameter calculated by the BJH method changes from 1.87 to 2.87 nm linearly as the alkyl chain length changes from C10 to C16, and the corresponding pore volume varies linearly with the surfactant chain length. This indicates that the pore diameter and pore volume can be precisely controlled by using the preparation method described in this work. The volume of mesopores, defined as the pores with diameter less than 10 nm, also shows a linear dependence on the surfactant chain length, as shown in the inset of Figure 1a. Lim et al.[4] suggested this control of pore diameter as a potential tool for controlling the diameter of carbon nanotubes produced in the pore system of these catalytic template materials.

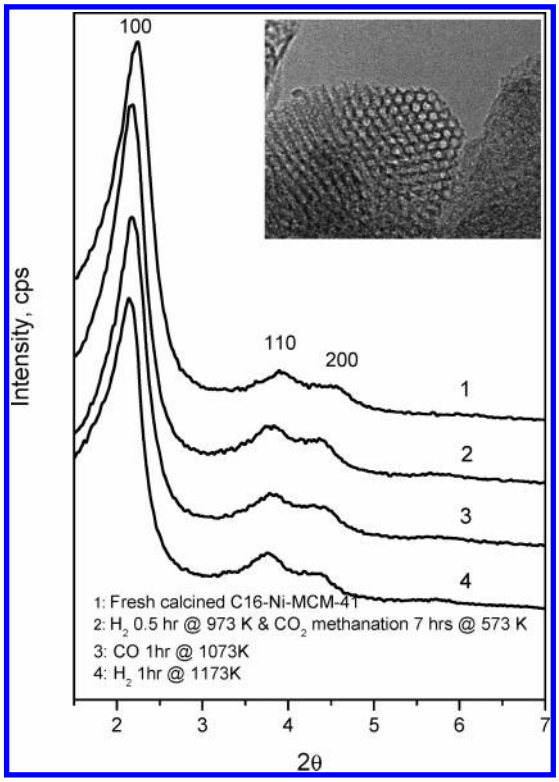

Figure 2. X-ray diffraction results of C16-Ni-MCM-41 sample, fresh and under different reaction conditions (inset: HR-TEM image of freshly calcined C16-Ni-MCM-41).

X-ray diffraction is one of the most important techniques for characterizing the structure of crystalline or other ordered materials. It has been widely used in the study of MCM-41 materials to complement the nitrogen physisorption because of its capability of assessing the two-dimensional hexagonal structure of the sample. In MCM-41 samples, the XRD peaks do not result from local order in the atomic range, but from the ordered channel walls. All C10−C16 samples were characterized by XRD to confirm the hexagonal structure of MCM-41; a typical XRD pattern is illustrated in Figure 2. As expected

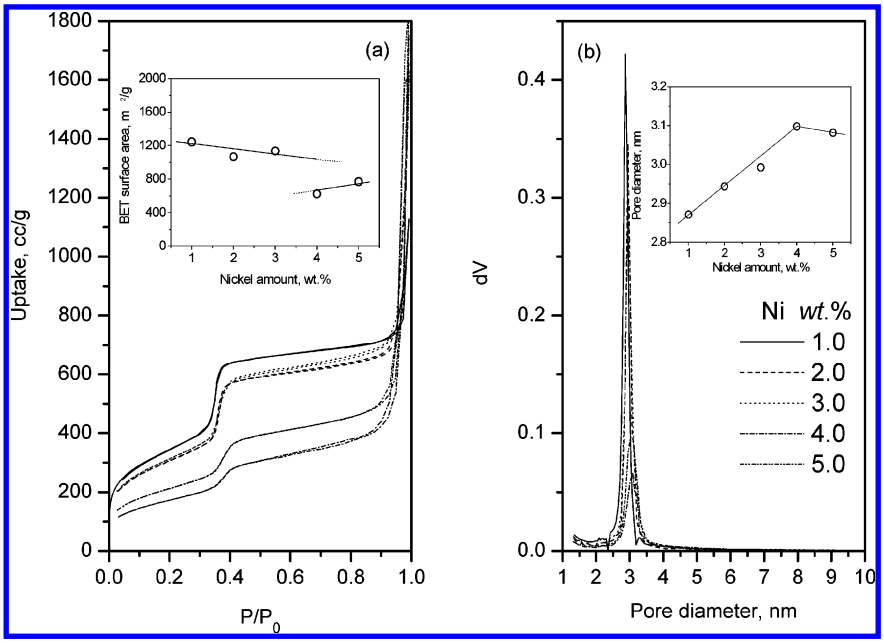

Figure 3. Nitrogen physisorption results of C16-Ni-MCM-41 samples with different nickel concentrations: (a) adsorption/desorption isotherms (inset: correlation of BET surface area with the nickel amount) and (b) pore size distribution (inset: correlation between the pore diameter and the nickel amount).

from the nitrogen physisorption results, a well-ordered two-dimensional hexagonal structure is observed, which gives a sharp (100) plane diffraction peak and the diffraction peaks of higher Miller Index planes, (110), (200), and (210). The HR-TEM image in the inset of Figure 2 shows clean long-range order of pore entrances, confirming the highly ordered hexagonal structure of the Ni-MCM-41 samples we prepared.

To determine how the incorporation of nickel affects the structure of MCM-41, a series of Ni-MCM-41 samples (1.0−5.0 wt %) were synthesized and characterized by nitrogen physisorption. Dzwigaj et al.[36] claimed that up to a certain amount of metal, the incorporation will improve the structure of the silica polymer by knitting the defects, which results in a pore diameter increase because of either larger transition element ion size or greater metal oxygen bond length while the unimodal pore size distribution is maintained. Figure 3 shows the nitrogen physisorption isotherms and pore size distributions of Ni-MCM-41 samples with different nickel content. Sharp capillary condensation, high adsorption volume, and unimodal pore size distribution remained substantially the same over the range of source metal concentration in our experiments by means of the so-called knitting effect. XRD results, not shown here, also confirm the highly ordered structure as well. The pore diameter is increased by 0.1 nm compared with a siliceous MCM-41 sample and increases linearly with the addition of nickel in the framework of MCM-41. This implies that the nickel species did not block the pore structure and was incorporated into the framework of silica. From the isotherms we observe that the slope of capillary condensation, which is a good estimate of structural order,[7] becomes smaller when the source nickel concentration increases in the original synthesis mixture, and the pore size distribution peak becomes broader, which means that the increased addition of nickel causes some loss of Ni-MCM-41 structure. Meanwhile, the pore diameter and BET surface area decrease for the sample with 5.0 wt % nickel, therefore, the maximum amount of nickel that can be incorporated in the MCM-41 framework using the current procedure preserving a good structural order is about 4.0 wt %, which is substantially similar to that of Co-MCM-41.

Reducibility of the Co incorporated into the MCM-41 framework has been related to the activity and the selectivity of SWNTs synthesis,[29] and is also expected to play an important role in CO_2 methanation. Understanding the reduction behavior of nickel in Ni-MCM-41 is, therefore, essential for the development of catalysts for these reactions. Temperature-programmed reduction (TPR) is a very convenient technique for studying the reduction behavior of supported oxide catalysts qualitatively. In this study, TPR was carried out in the temperature range from 323 to 1173 K for the purpose of investigating the reduction behavior of the nickel species in Ni-MCM-41 as a stability index. TPR patterns of C16-Ni-MCM-41 sample are compared in Figure 4 with reference compounds and impregnated Ni/MCM-41. The Ni-MCM-41 sample does not show any reduction below 800 K, which suggests the presence of nickel oxides and nickel nitrate compounds on the silica surface can be ruled out. Compared to the impregnated Ni/MCM-41 sample, Ni-MCM-41 prepared hydrothermally has much higher stability against reduction reflected in a higher reduction temperature, which indicates the nickel species are entirely incorporated into the silica framework, as observed for cobalt elsewhere.[4] Nickel is completely reduced after holding the temperature constant at 1200 K for 1 h, and pulled out of the framework on the pore wall surface. Once it is exposed to air at 773 K it can be reoxidized to create nickel oxide on the surface of the silica walls. It is observed that the second and subsequent runs show different patterns compared to the first TPR run. They have clear shoulders on the high temperature side of the reduction peak, which are due to nickel oxide interaction with the silica wall to form nickel silicate easily at high temperature.[37] However, as the TPR and reoxidation cycles of Ni-MCM-41 are repeated, the interaction between nickel oxide and the silica wall is weaken by the further reduction of nickel silicate. Therefore, the high temperature shoulder of the reduction peak becomes smaller and smaller, and approaches that of the TPR pattern of nickel oxide.

The TPR profiles for samples having the same nickel content but different pore diameter are shown in Figure 5. Unlike the Co-MCM-41 samples, in which the radius of curvature of the

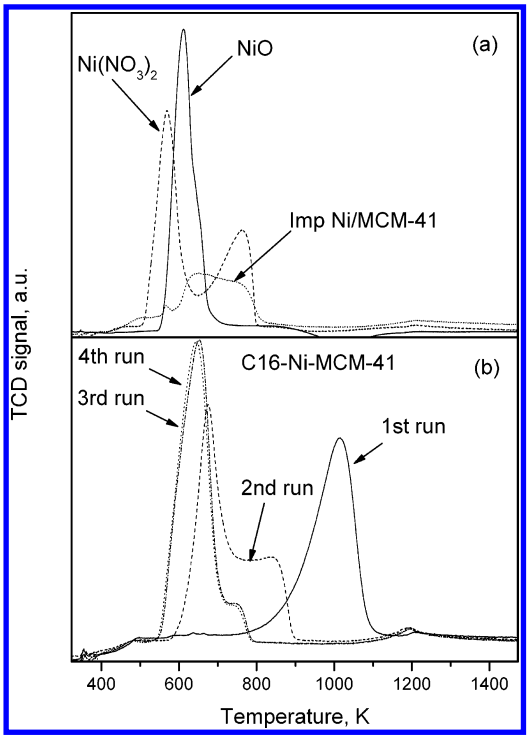

Figure 4. H_2 temperature-programmed reduction (TPR) profiles of (a) C16-Ni-MCM-41 and (b) impregnated Ni/C16-MCM-41 and reference compounds.

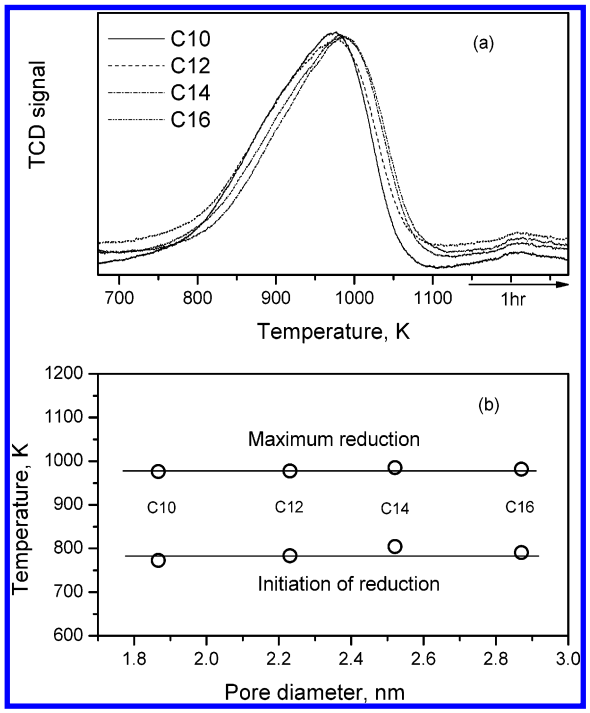

Figure 5. H_2 temperature-programmed reduction profiles of Ni-MCM-41 with the same nickel amount but different pore diameters: (a) TPR patterns of C10−C16 MCM-41 with constant nickel loading and (b) temperature of maximum reduction and initiation of reduction as a function of pore diameter.

pores strongly affects reducibility of the Co, reduction of Ni-MCM-41 samples in this study did not show any correlation with the pore diameter. All the samples have a similar temperature at the maximum reduction rate (summit of the reduction peak) regardless of the pore size. In addition, both the temperature at the maximum reduction rate and the temperature of reduction initiation are plotted as a function of

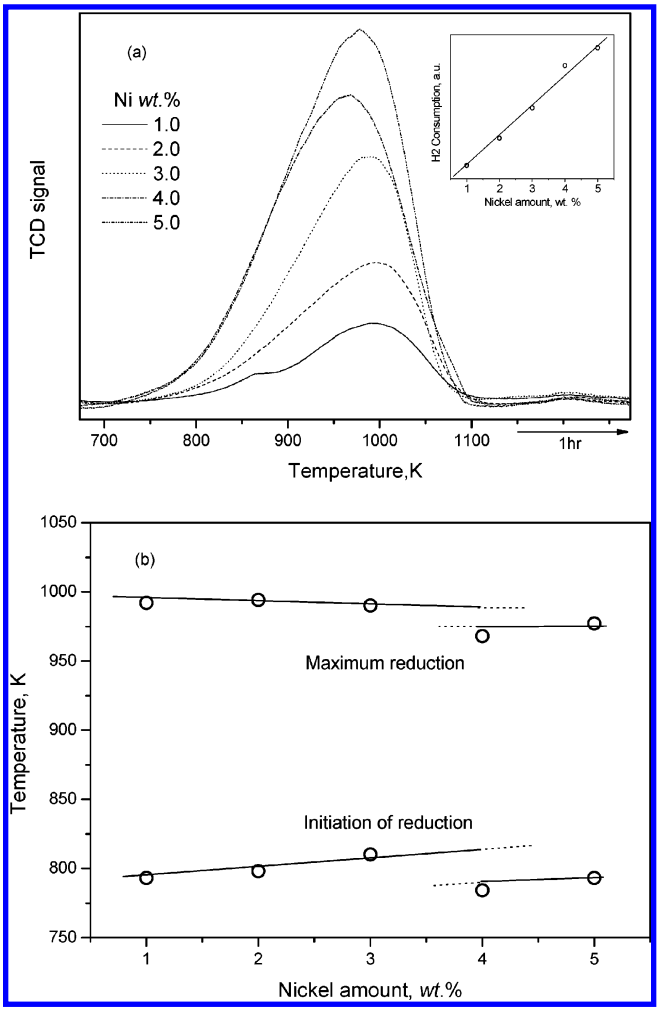

Figure 6. H_2 temperature-programmed reduction profiles of C16-Ni-MCM-41 with different nickel loadings: (a) TPR patterns of C16-MCM-41 with different nickel loading (inset: correlation of hydrogen consumption with nickel amount) and (b) temperature of maximum reduction and initiation of reduction as a function of nickel loading.

pore diameter. It is observed that the pore radius of curvature has a small effect, if any, on the reduction initiation or maximum rate, as shown in Figure 5b.

TPR experiments were conducted on C16-Ni-MCM-41 samples with different nickel loadings. Reduction peak area increases linearly with the increase of nickel content without showing reduction of surface nickel oxide at low temperature (<700 K), implying the nickel species are incorporated into the silica framework regardless of the Ni loading. These results, and those obtained for the reduction of Ni-MCM-41 samples with 1 wt % loading but of different pore diameter, show the metal loading up to 4 wt % and the pore diameter, observed to affect the reducibility of Co incorporated in MCM-41, have a less dramatic effect on the reducibility of Ni-MCM-41. When the nickel loading increases beyond 4 wt %, however, both initial reduction and the maximum reduction rate temperatures shift to a lower value. The higher nickel loading results in a higher nickel concentration close to the subsurface, which makes the reduction easier.

Lim et al.[1] proposed that in Co-MCM-41, where some of the Si ions are substituted by Co ions, the smaller oligomer silica ring structure in small pores is more difficult to break than that in larger rings in larger pores, thus resulting in a higher reduction temperature for cobalt incorporated in smaller pore diameter MCM-41. Nickel, as the next neighbor element to

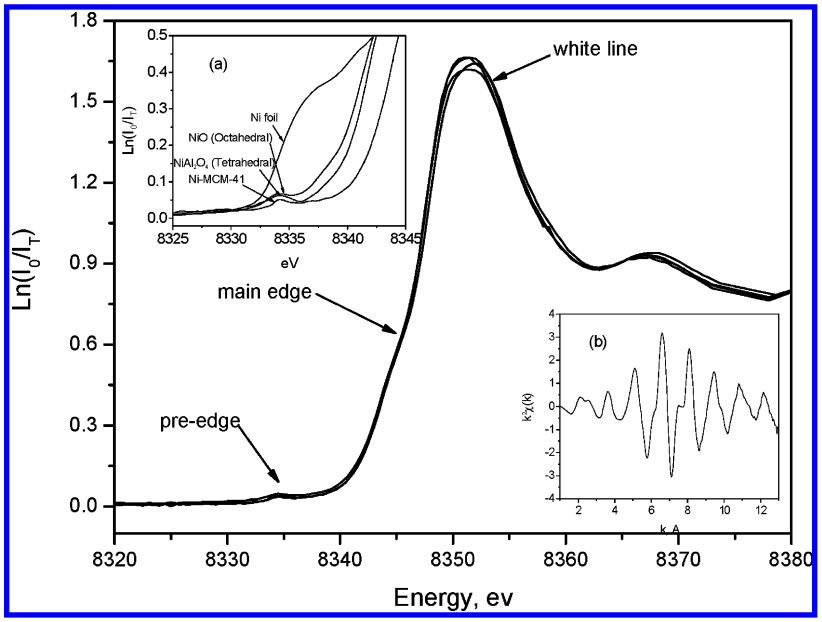

Figure 7. XANES spectra of C10−C16 Ni-MCM-41: (inset a) comparison of preedge feature with reference compounds; (inset b) spectra in k^2-weighted k space.

cobalt, is expected to have a local environment similar to cobalt in the framework of MCM-41. Thus, the radius of curvature should have a similar effect on the reduction of nickel according to Lim's assumption. The thermodynamics of reduction can also predict under which conditions a catalyst can be reduced, i.e., the reduction will proceed when the change in Gibbs free energy has a negative value, which depends on the partial pressure ratio of water to hydrogen. Expression 1 shows how ΔG depends on pressures and temperature:[38]

$$\Delta G = nRT \ln\left[\left(\frac{p_{H_2O}}{p_{H_2}}\right)\Big/\left(\frac{p_{H_2O}}{p_{H_2}}\right)_{eq}\right] \quad (1)$$

with the subscript "eq" defined for the ratio at equilibrium. The partial pressure ratio of water to hydrogen for both cobalt and nickel reduction will be the same under the same reduction condition due to the same carrier gas flow rate and same efficiency of removing water. On the other hand, the pressure ratio of nickel at equilibrium is 10 times larger than that of cobalt. This makes the reduction of nickel much easier and faster than that of cobalt. The inhibition of smaller silica rings is relatively weaker for Ni compared to Co.

The first-row transition elements have well-defined site symmetry spectra in X-ray absorption near edge structure (XANES) measurements.[38] The XANES preedge peak is attributed to the 1s−3d transition. Figure 7 illustrates the XANES spectra of nickel-incorporated MCM-41 synthesized with different alkyl chain lengths, from C10 to C16. All samples show almost identical preedge features. This indicates that these samples have identical nickel ion species even though the alkyl chain length (pore diameter) is different. Compared with the model compounds shown in Figure 7, inset (a), the nickel ions have a similar preedge feature to that of nickel aluminate, which contains a mixture of tetrahedrally and octahedrally coordinated species confirmed by XRD (not shown here). Therefore, this suggests that the nickel in MCM-41 may consist of a mixture of tetrahedral and octahedral local structures, or more likely a mixture of tetrahedral and distorted tetrahedral local symmetry. It is hard to tell, based on this evidence, whether the local symmetry of nickel ions is tetrahedral or octahedral. However, the EXAFS results will later confirm that the nickel ions are coordinated distorted tetrahedrally, because the Ni−O coordination number is close to 4. On the basis of the earlier characterization results (TPR), all Ni ions are believed to be incorporated in the silica framework having distorted tetrahedral coordination with surrounding oxygen anions.

TABLE 1: Ni−O Coordination Numbers of Hydrated and Dehydrated Ni-MCM-41 Samples

	Ni−O coordination no.			
	C10 Ni-MCM-41	C12 Ni-MCM-41	C14 Ni-MCM-41	C16 Ni-MCM-41
hydrated	5.58	5.04	6.04	5.02
dehydrated	4.42	4.30	−	3.98

At the time that EXAFS was introduced in catalysis, around 1975, the technique was considered to be one of the most promising tools for investigating catalysts. It gives detailed local structure information, such as the coordination number, bond length, etc. Detailed information on data analysis of EXAFS and XANES may be found elsewhere.[39] Figure 7, inset (b), shows the EXAFS spectra in k^2-weighted k space (k is the photoelectron wavenumber). Good spectra can be recorded up to $k = 13$ Å^{-1}, which makes the fitting and calculation reliable. The average first-shell Ni−O coordination numbers for both hydrated and dehydrated samples are listed in Table 1. All dehydrated samples show Ni−O coordination numbers between 3.98 and 4.42, giving evidence again that the Ni ions have tetrahedral coordination with the surrounding oxygen anions and are substituted for Si ions in the framework. On the other hand, hydrated samples show higher Ni−O coordination numbers, between 5 and 6, which may be attributed to water molecules contacting directly the Ni centers to make pseudooctahedral species, as Lim et al. [1] proposed for cobalt-substituted MCM-41 catalysts.

In situ XANES TPR experiments were carried out as complementary experiments to hydrogen TPR. The temperature was ramped from room temperature to 973 K at 20 K/min, continuously monitoring the state of the Ni in the Ni-MCM-41 sample. It is clearly shown in Figure 8 that the intensity of the white line drops and the preedge peak intensity increases during the reduction. Ciuparu et al.[39] claimed that the preedge peak intensity and white line intensity could be selected as the main

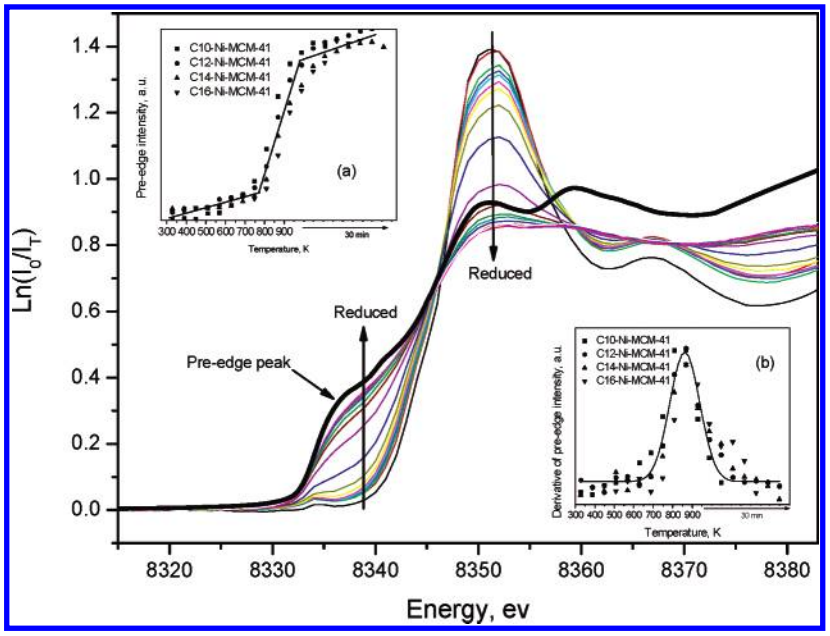

Figure 8. XANES spectra of in situ H_2 temperature-programmed reduction of C12-Ni-MCM-41: (inset a) preedge peak intensity of C10−C16 Ni-MCM-41 as a function of temperature; (inset b) derivative of preedge peak intensity of C10−C16 Ni-MCM-41 as a function of temperature.

features to monitor the reduction of cobalt in Co-MCM-41, therefore, the preedge peak intensity was chosen in the present work to characterize the change of nickel in our Ni-MCM-41 samples. The results were compared with hydrogen TPR under 5% H_2/Ar atmosphere, where a lower reduction temperature was expected because ultrahigh purity hydrogen was used during the in situ XANES TPR experiments. All the samples have identical trends of the preedge peak intensity, regardless of the alkyl chain length from C10 to C16, which demonstrates that C10−C16 Ni-MCM-41 samples follow the same reduction pathway. The reduction of the entire sample series start from approximately the same temperature (780 K), shown in inset (a) of Figure 8, which is consistent with the 5% hydrogen reduction results. One possible reason for this consistency is that nickel may be reduced only above a certain temperature thermodynamically in a pure hydrogen environment. The derivative of the preedge peak intensity was taken to obtain a more readable TPR profile of Ni-MCM-41 as shown in inset (b) of Figure 8. All the samples have similar TPR patterns, which is consistent with the low concentration hydrogen TPR regardless of the pore diameter of Ni-MCM-41. As expected, the major difference is that the temperature of maximum reduction rate of high concentration H_2-TPR shifts 100 K lower than that of the low concentration H_2-TPR. This is most likely because nickel can be reduced faster under higher hydrogen partial pressure.

Highly dispersed nickel nanoparticles are essential for obtaining good catalytic activity and selectivity during the SWNT synthesis and hydrogenation of CO_2 to methane. In situ H_2 reductions at different temperatures were performed to correlate the Ni state with the reduction temperature. The C16-Ni-MCM-41 samples were reduced under ultrahigh purity hydrogen for 30 min at 673, 773, 873, and 973 K, respectively. The EXAFS spectra were collected at room temperature after each of the reduction experiments performed with Ni-MCM-41 samples of different reduction temperature and were used to determine the average first shell Ni−Ni and Ni−O coordination numbers. Figure 9 shows the preedge feature and white line feature of Ni-MCM-41 samples reduced at different temperatures, compared with the fresh sample and the nickel foil. Compared to the fresh sample, 673 and 773 K reductions decrease the white line intensity significantly but do not exhibit a metallic preedge feature. A possible explanation is that only dehydroxylation happened on the surface; 2 OH^- ligands have been replaced by O^{2-} ligands in the coordination sphere of nickel. It is mostly the change in electon donation (greater for O^{2-} than for 2 OH^-) that decreases the white line, but the nickel atoms are not reduced significantly and there is no significant change of the preedge feature. Clear reduction of nickel can be observed at 873 K, compared with the fresh sample. The white line continued to decrease and the preedge peak intensity to increase. Nickel atoms migrate quickly to form nickel particles and a growing metallic preedge feature is observed. Most of the nickel has been reduced under more severe reduction temperature (973 K). Calculated first shell Ni−Ni and Ni−O coordination numbers are illustrated in Table 2. The Ni−Ni coordination number increases systematically from 2.86 to 7.62 with increasing reduction temperature from 673 to 973 K. On the other hand, the Ni−O coordination number decreases linearly from 3.98 in fresh sample to 0.48, which is from tetrahedral coordination with the oxygen to almost complete reduction.

TABLE 2: Ni−Ni and Ni−O Coordination Numbers of C16-Ni-MCM-41 Samples Reduced at Different Temperatures

	coordination no. at reduction temp (K) =				
	fresh	673	773	873	973
Ni−Ni		2.86	3.46	5.65	7.62
Ni−O	3.98	3.13	2.30	0.95	0.48

Stability of C16-Ni-MCM-41 Template after SWNT Synthesis and CO_2 Methanation. The stability of C16-Ni-MCM-41 was tested for CO disproportionation to synthesize SWNT and for hydrogenation of CO_2 to methane. Figure 10 shows the Raman spectrum of C16-Ni-MCM-41 sample after CO disproportionation, along with the TEM image as an inset. The TEM image gives clear evidence that the single wall carbon nanotubes grow out of the Ni-MCM-41 catalytic template. The presence of characteristic features for the Raman breathing mode (RBM) at 253 cm^{-1} and the peak complex centered around 1580 cm^{-1} suggest the presence of SWNT with rather narrow distribution of diameters. A more detailed characterization of the catalytic performance of the Ni-MCM-41 catalyst for SWNT

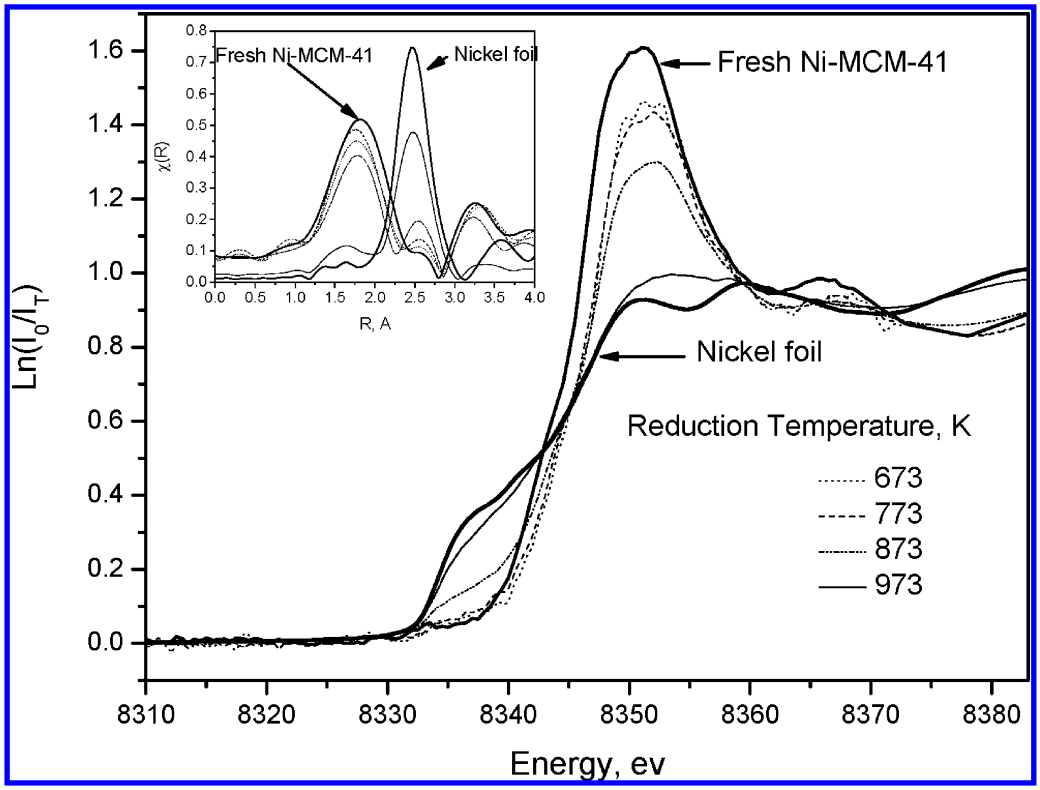

Figure 9. XANES spectra of H_2 reduction of C16-Ni-MCM-41 sample at different temperatures (inset: spectra in R space).

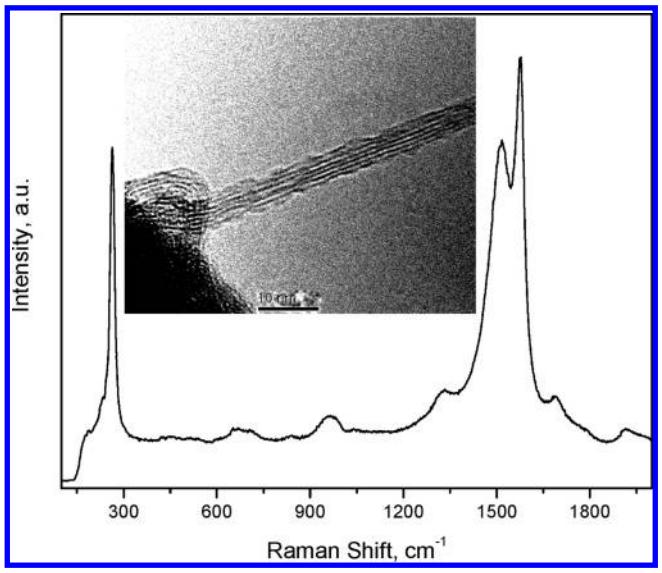

Figure 10. Raman spectrum showing the presence of SWNT (inset: TEM micrograph confirmation).

TABLE 3: CO_2 Methanation with C16-Ni-MCM-41

	conversion %		selectivity %	
H_2:CO_2:He	H_2	CO_2	CO	CH_4
4:1:45	13.2	12.4	30.6	69.4
4:1:7.5	3.7	4.2	31.4	68.6

synthesis, which is beyond the purpose of this contribution, is given elsewhere.[31]

Preliminary results of CO_2 methanation at 573 K with different reactant concentrations can be found in Table 3. It is observed that the selectivity of methane is about 70%, which indicates that the Ni-MCM-41 is a good catalyst for CO_2 methanation. This selectivity does not change dramatically with the increase of reactant concentration. The conversion of hydrogen and CO_2 are around 13%, and drops to about 4% at higher reactant concentration due to the short contact time of reactant gas. Figure 11 shows the nitrogen physisorption isotherm of the fresh calcined sample compared to those after CO disproportionation and after CO_2 methanation. Apparently, structural order decreases after both catalytic reactions; the

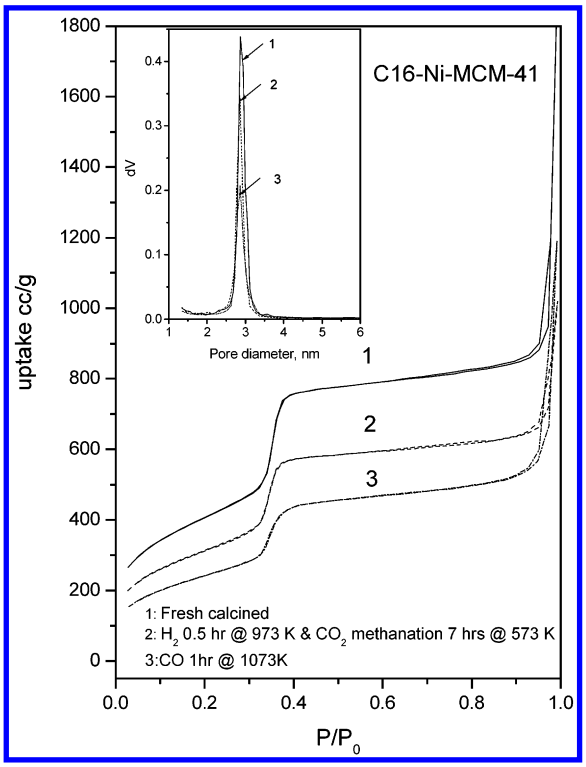

Figure 11. Nitrogen physisorption results of C16-Ni-MCM-41 sample exposed to different reaction conditions (inset: pore size distribution profile of C16-Ni-MCM-41 sample exposed to different reaction conditions).

TABLE 4: Physical Properties of C16-Ni-MCM-41 Samples Exposed to Different Reaction Conditions

treatment	BET, m^2/g	pore diameter, nm	mesopore vol, cm^3/g	total pore vol, cm^3/g	slope of capillary ondensation, au	fwhm, nm
fresh calcined	1478	2.86	1.294	3.043	7332	0.18
CO disproportionation 1 h @ 1073 K	883	2.86	0.773	1.919	3475	0.21
H_2 reduction 0.5 h @ 913K and CO_2 methanation 7 h @ 573K	1139	2.86	1.005	1.663	5707	0.18

adsorption volume decreases compared with the fresh sample. However, a highly ordered structure has been maintained even under these severe reaction conditions. Isotherms still show clear and sharp capillary condensation after reaction and the pore size distributions, calculated by the BJH method, show a narrow single distribution peak, which indicates good stability of nickel substituted MCM-41 catalysts prepared following the procedure described in this work.

Physical properties of C16-Ni-MCM-41 before and after catalytic reaction are listed in Table 4. Fresh samples show identical average pore diameter with the catalysts after reaction (analyzed before SWNT removal from the catalyst, which means the residues from the catalytic reactions (i.e. the SWNT) did not block the pore structure. However, the catalytic reactions may affect porosity and/or surface area. The BET surface area, slope of the capillary condensation, and full width at half-maximum (fwhm) of pore size distribution are selected as quantitative measures of the physical structure. Compared to fresh calcined samples, the BET surface area and slope of capillary condensation drop by about one-third after CO disproportionation; the fwhm increases about 17%. The Ni-MCM-41 sample shows better physical stability under CO_2 methanation than under CO disproportionation, most likely because of the milder reaction conditions.

XRD experiments were also performed to test the structural stability of C16-Ni-MCM-41 catalysts under different reaction conditions, as shown in Figure 2. The XRD patterns illustrate that the C16-Ni-MCM-41 sample still preserves its good hexagonal structure even under harsh reaction conditions, for instance, the carbon deposition, hydrogenation of CO_2, and complete reduction with hydrogen at 1173 K. Calculation of pore wall thickness demonstrates that the pore wall thickness does not change after different reactions, which is essential to maintain the long-range order of the structure of MCM-41.

Conclusions

Highly ordered and reproducible Ni-MCM-41 samples were prepared by a hydrothermal method. Similar to the Co-MCM-41 samples, the pore diameter and porosity can be precisely controlled by changing the surfactant chain length.[4] Nickel was incorporated into the silica framework successfully and highly dispersed, which makes the Ni-MCM-41 a stable catalyst in either CO disproportionation or CO_2 methanation. X-ray absorption spectroscopy results indicate that the overall local environment of nickel was a tetrahedral or distorted tetrahedral coordination with surrounding oxygen anions. Hydrogen TPR revealed that our Ni-MCM-41 samples have high stability against reduction. However, compared to Co-MCM-41, the Ni-MCM-41 catalysts have lower reduction temperatures, and both the H_2-TPR and in situ XANES TPR reveal that the reducibility of nickel has no clear correlation with the pore radius of curvature. This is probably a result of nickel being thermodynamically easier to reduce than cobalt. The growth of SWNT in the pores of Ni-MCM-41was confirmed by TEM and Raman spectroscopy. Ni-MCM-41 shows high selectivity to methane tested by catalytic hydrogenation of CO_2. Our Ni-MCM-41 samples show high stability during catalytic reactions and the nickel particle size can be controlled by using different prereduction temperatures.

Acknowledgment. We are grateful to the DOE, Office of Basic Energy Sciences, for financial support. We also thank NSLS Brookhaven National Laboratory for synchrotron X-ray beam time.

References and Notes

(1) Lim, S.; Ciuparu, D.; Chen, Y.; Yang, Y. H.; Pfefferle, L.; Haller, G. L. *J. Phys. Chem. B* **2005**, *109*, 2285.

(2) Beck, J. S.; Vartuli, J. C.; Roth, W. J.; Leonowicz, M. E.; Kresge, C. T.; Schmitt, K. D.; Chu, C. T. W.; Olson, D. H.; Sheppard, E. W.; McCullen, S. B.; Higgins, J. B.; Schlenker, J. L. *J. Am. Chem. Soc.* **1992**, *114*, 10834.

(3) Kresge, C. T.; Leonowicz, M. E.; Roth, W. J.; Vartuli, J. C.; Beck, J. S. *Nature* **1992**, *359*, 710.

(4) Lim, S.; Ciuparu, D.; Pak, C.; Dobek, F.; Chen, Y.; Harding, D.; Pfefferle, L.; Haller, G. *J. Phys. Chem. B* **2003**, *107*, 11048.

(5) Yang, Y. H.; Lim, S. Y.; Wang, C. A.; Du, G. A.; Haller, G. L. *Microporous Mesoporous Mater.* **2004**, *74*, 133.

(6) Pak, C.; Haller, G. L. *Microporous Mesoporous Mater.* **2001**, *48*, 165.

(7) Yang, Y. H.; Lim, S.; Wang, C.; Harding, D.; Haller, G. *Microporous Mesoporous Mater.* **2004**, *67*, 245.

(8) Konovalova, T. A.; Gao, Y. L.; Schad, R.; Kispert, L. D.; Saylor, C. A.; Brunel, L. C. *J. Phys. Chem. B* **2001**, *105*, 7459.

(9) Hartmann, M.; Poppl, A.; Kevan, L. *J. Phys. Chem.* **1996**, *100*, 9906.

(10) Kunisada, N.; Choi, K. H.; Korai, Y.; Mochida, I. *Appl. Catal., A* **2004**, *260*, 185.

(11) Li, X.; Wang, A. J.; Sun, Z. C.; Li, C.; Ren, J.; Zhao, B.; Wang, Y.; Chen, Y. Y.; Hu, Y. K. *Appl. Catal., A* **2003**, *254*, 319.

(12) Wojcieszak, R.; Monteverdi, S.; Mercy, M.; Nowak, I.; Ziolek, M.; Bettahar, M. M. *Appl. Catal., A* **2004**, *268*, 241.

(13) Lewandowska, A.; Monteverdi, S.; Bettahar, M.; Ziolek, M. *J. Mol. Catal. A: Chem.* **2002**, *188*, 85.

(14) Parvulescu, V.; Su, B. L. *Catal. Today* **2001**, *69*, 315.

(15) Parvulescu, V.; Anastasescu, C.; Constantin, C.; Su, B. L. Highly selective oxidation of aromatic hydrocarbons (Styrene, Benzene and Toluene) with H_2O_2 over Ni, Ni−Cr and Ni−Ru modified MCM-41 catalysts. In *Impact of Zeolites and Other Porous Materials on the New Technologies at the Beginning of the New Millennium*, Parts a and B; Elsevier: Boston, MA, 2002; Vol. 142, p 1213.

(16) Parvulescu, V.; Dascalescu, C.; Su, B. L. Highly selective oxidation of styrene with hydrogen peroxide catalyzed by mono- and bimetallic (Ni, Ni−Cr and Ni−Ru) incorporated MCM-41 silicas. In *Nanotechnology in Mesostructured Materials*; Elsevier, New York, 2003; Vol. 146, p 629.

(17) Chang, F. W.; Hsiao, T. J.; Chung, S. W.; Lo, J. J. *Appl. Catal., A* **1997**, *164*, 225.

(18) Aksoylu, A. E.; Misirli, Z.; Onsan, Z. I. *Appl. Catal., A* **1998**, *168*, 385.

(19) Aksoylu, A. E.; Onsan, Z. I. *Appl. Catal., A* **1998**, *168*, 399.

(20) Constantin, C.; Parvulescu, V.; Bujor, A.; Popescu, G.; Su, B. L. *J. Mol. Catal. A: Chem.* **2004**, *208*, 245.

(21) Parvulescu, V.; Constantin, C.; Popescu, G.; Su, B. L. *J. Mol. Catal. A: Chem.* **2004**, *208*, 253.

(22) Seidel, R.; Duesberg, G. S.; Unger, E.; Graham, A. P.; Liebau, M.; Kreupl, F. *J. Phys. Chem. B* **2004**, *108*, 1888.

(23) Konya, Z.; Vesselenyi, I.; Kiss, J.; Farkas, A.; Oszko, A.; Kiricsi, I. *Appl. Catal., A* **2004**, *260*, 55.

(24) Zhang, M.; Yudasaka, M.; Iijima, S. *J. Phys. Chem. B* **2004**, *108*, 149.

(25) Yudasaka, M.; Kikuchi, R.; Ohki, Y.; Ota, E.; Yoshimura, S. *Appl. Phys. Lett.* **1997**, *70*, 1817.

(26) Andriotis, A. N.; Menon, M.; Froudakis, G. *Phys. Rev. Lett.* **2000**, *85*, 3193.

(27) Saito, Y. *Jpn. J. Appl. Phys., Part 2* **1994**, *33*, L526.

(28) Jia, J.; Wang, Y.; Tanabe, E.; Shishido, T.; Takehira, K. *Microporous Mesoporous Mater.* **2003**, *57*, 283.
(29) Ciuparu, D.; Chen, Y.; Lim, S.; Haller, G. L.; Pfefferle, L. *J. Phys. Chem. B* **2004**, *108*, 503.
(30) Lensveld, D. J.; Mesu, J. G.; van Dillen, A. J.; de Jong, K. P. The application of well-dispersed nickel nanoparticles inside the mesopores of MCM-41 by use of a nickel citrate chelate as precursor. In *Scientific Bases for the Preparation of Heterogeneous Catalysts*; Elsevier: Amsterdam, The Netherlands, 2002; Vol. 143, p 647.
(31) Chen, Y.; Ciuparu, D.; Yang, Y. H.; Lim, S. Y.; Wang, C.; Haller, G. L.; Pfefferle, L. D. *Nanotechnology* **2005**, *16*, S476.
(32) Elshobaky, G. A.; Ghoneim, N. M.; Sultan, E. A. *Thermochim. Acta* **1983**, *63*, 39.
(33) Barrett, E. P.; Joyner, L. G.; Halenda, P. P. *J. Am. Chem. Soc.* **1951**, *73*, 373.
(34) Stern, E. A.; Newville, M.; Ravel, B.; Yacoby, Y.; Haskel, D. *Phys. B* **1995**, *209*, 117.
(35) Ankudinov, A. L.; Ravel, B.; Rehr, J. J.; Conradson, S. D. *Phys. Rev. B* **1998**, *58*, 7565.
(36) Dzwigaj, S.; Krafft, J. M.; Che, M.; Lim, S.; Haller, G. L. *J. Phys. Chem. B* **2003**, *107*, 3856.
(37) Louis, C.; Cheng, Z. X.; Che, M. *J. Phys. Chem.* **1993**, *97*, 5703.
(38) Niemantsverdriet, J. W. *Spectroscopy in Catalysis an Introduction*; VCH: New York, 1993.
(39) Ciuparu, D.; Chen, Y.; Lim, S.; Yang, Y. H.; Haller, G. L.; Pfefferle, L. *J. Phys. Chem. B* **2004**, *108*, 15565.